A New Heat Source Model for Keyhole Plasma Arc Welding in FEM Analysis of the Temperature Profile

The model takes into consideration keyhole configuration and decay of heat distribution along the workpiece thickness

BY C. S. WU, H. G. WANG, AND Y. M. ZHANG

ABSTRACT. It is a key issue to establish an appropriate model of the heat source in the simulation of keyhole plasma arc welding (PAW). It requires that the model account for the keyhole effect and have the characteristic of volumetric distribution along the direction of the plate thickness. For available heat source models, neither Gaussian nor double ellipsoidal modes of heat source is applicable to the keyhole PAW process. Considering the force of the high-speed plasma jet and the associated strong momentum, a modified three-dimensional conical heat source model is proposed as the basis for the numerical analysis of temperature fields in the keyhole PAW process. Further, a new heat source model for quasi-steady state temperature field in keyhole PAW is developed to consider the "bugle-like" configuration of the keyhole and the decay of heat intensity distribution of the plasma arc along the direction of the workpiece thickness. Based on this heat source model, finite-element analysis of the temperature profile in keyhole PAW was conducted and the weld geometry was determined. The results showed that the predicted location and locus of the melt-line in the PAW weld cross section are in good agreement with experimental measurements.

Introduction

Plasma arc welding (PAW) offers significant advantages over conventional gas tungsten arc welding (GTAW) in terms of penetration depth, joint preparation, and thermal distortion (Refs. 1, 2). The arc used in PAW is constricted by a small nozzle and has a much higher gas velocity (300–2000 m/s) and heat input intensity

C. S. WU and H. G. WANG are with the Institute for Materials Joining, Shandong University, Jinan, China. Y. M. ZHANG is with the Center for Manufacturing and Department of Electrical and Computer Engineering, University of Kentucky, Lexington, Ky.

$(10^9–10^{10}$ w/m²) than that in GTAW (gas velocity 80–150 m/s, heat input intensity $10^8–10^9$ w/m²) (Refs. 3, 4). As the plasma arc impinges on the area where two workpieces are to be joined, it can melt material and create a molten liquid pool. Because of its high velocity and the associated momentum, the arc can penetrate through the molten pool and form a hole in the weld pool, which is usually referred to as a keyhole (Ref. 5). Moving the welding torch and the associated keyhole will cause the flow of the molten metal surrounding the keyhole to the rear region where it resolidifies to form a weld bead.

The keyhole mode of welding is the primary attribute of high-power density welding processes (PAW, laser welding, and electron beam welding), which makes them penetrate thicker pieces with a single pass. Compared to laser welding and electron beam welding, keyhole PAW is more cost effective and more tolerant of joint preparation, though its energy is less dense and its keyhole is wider (Ref. 4).

Thus, keyhole PAW has found applications on the welding of many important structures (Refs. 6–14). Although keyhole PAW has the potential to replace GTAW in many applications as a primary process for precise joining (Ref. 1), the stable state of the keyhole is an important issue in applying PAW (Ref. 15). In keyhole PAW, the quality of the weld depends on the keyhole stability, which itself depends on a large number of factors, especially the physical characteristics of the material to be

welded and the welding process parameters to be used (Ref. 5). Thus, keyhole PAW is susceptible to the variation of welding process parameters, which makes it have a narrower range of applicable process parameters for good weld quality so that keyhole PAW is still limited in its wide application in industry (Ref. 16). The temperature profile around the weld pool has great influence on the formation and stability of keyhole. Through numerical simulation of the temperature field and the weld pool behavior in keyhole PAW, the process parameters can be optimized for obtaining high-quality of weld structure. Therefore, it is of great significance to model and simulate the temperature distribution and weld pool geometry in the keyhole PAW process.

The key issue for numerical analysis of temperature field in keyhole plasma arc welding is how to develop a heat source model that reflects the thermo-physical characteristics of the keyhole PAW process. Because of the complexity of the phenomena associated with the formation of a keyhole, only a limited number of theoretical studies treating the PAW process have been reported, each of varying degrees of approximation, and each focusing on different aspects of the problem (Refs. 11, 17–21). General Gaussian or double-ellipsoidal heat source models used widely in simulation of arc welding processes are not suitable for keyhole PAW. As the first step in a series of study, this paper focuses on developing a suitable heat source model for finite-element analysis of temperature profile in keyhole PAW.

Models of Heat Source in Keyhole PAW

As mentioned above, the key problem in FEM analysis of keyhole PAW is how to model the welding heat source. Most researchers employed a Gaussian distribution of heat flux (W/m²) deposited on the sur-
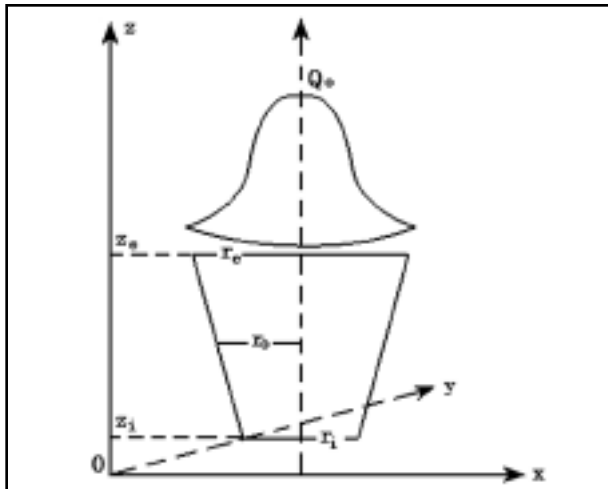
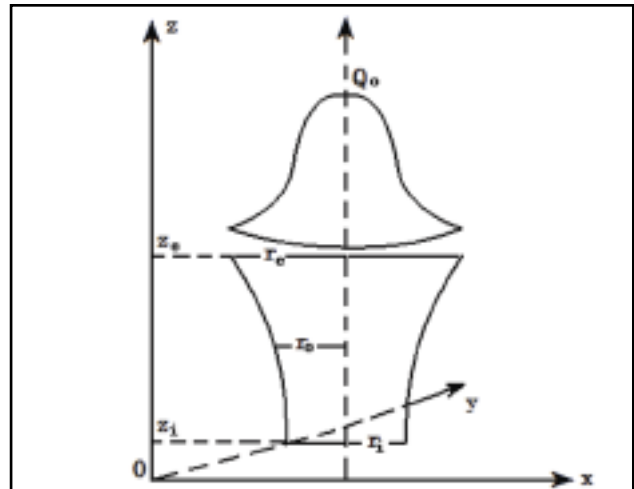*Fig. 1 — Schematic of TDC model.*

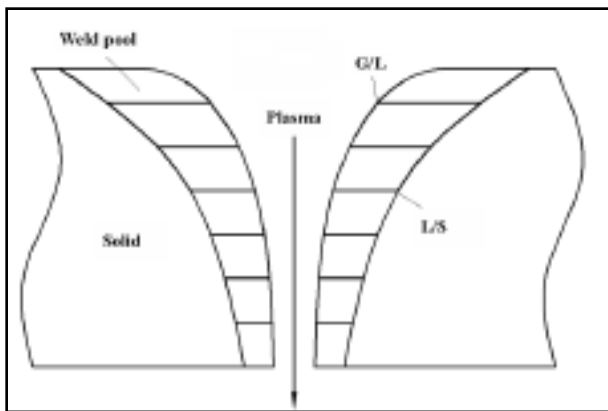*Fig. 2 — Schematic of MTDC model.*

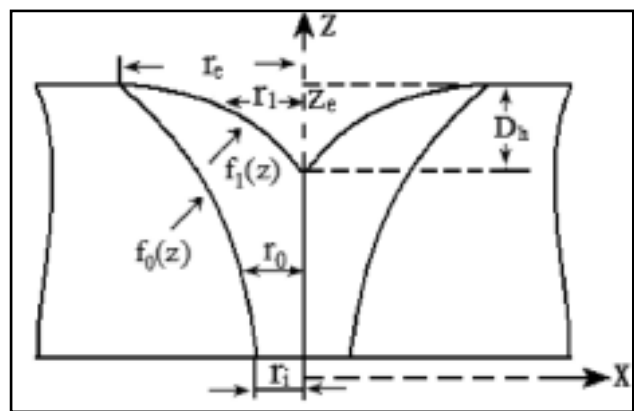*Fig. 3 — Schematic of keyhole and weld pool.*

Fig. 4 — Schematic of QPAW model.

face of the workpiece (Refs. 22–24). Although such a surface mode of heat source may be used for the shallow penetration arc welding processes like GTAW, it does not reflect the action of arc pressure on the weld pool surface so that it is not suitable for modeling the welding processes with deeper penetration like gas metal arc welding (GMAW). Goldak proposed a double-ellipsoidal heat source model, which has the capability of analyzing the thermal history of deep penetration welds like GMAW (Ref. 25). However, the double-ellipsoidal distribution of heat intensity (W/m^3) is still not applicable to the high-density welding processes with high ratio of the weld penetration to width, such as keyhole PAW (Ref. 26). Keyhole PAW produces a weld with high ratio of depth to width. The cross section of the weld is of the "bugle-like" configuration. To consider the strong action of the plasma jet and the resulted bugle-like weld configuration in keyhole PAW, new types of welding heat source models must be proposed.

Three-Dimensional Conical Heat Source

Three-dimensional conical heat source (TDC) is a volumetric heat source that considers the heat intensity distribution along the workpiece thickness. As shown in Fig. 1, the heat intensity deposited region is maximum at the top surface of workpiece, and is minimum at the bottom surface of workpiece. Along the thickness of the workpiece, the diameter of the heat density distribution region is linearly decreased. But the heat density at the central axis (z-direction) is kept constant. At any plane perpendicular to z-axis, the heat intensity is distributed in a Gaussian form. Thus, in fact, TDC is the repeated addition of a series of Gaussian heat sources with different distribution parameters and the same central maximum values of heat density along the workpiece thickness. In this way, the heating action of the plasma jet through the workpiece in keyhole PAW is considered.

At any plane perpendicular to the z-axis, the heat intensity distribution may be written as

$$Q_V(r,z) = Q_0 \exp\left(-\frac{3r^2}{r_0^2}\right) \qquad (1)$$

where Q_0 is the maximum value of heat intensity, r_0 is the distribution parameter, and r is the radial coordinate. The key problem is how to determine the parameters Q_0 and r_0.

As shown in Fig. 1, the height of the conical heat source is $H = z_e - z_i$, the z-coordinates of the top and bottom surfaces are z_e and z_i, respectively, and the diameters at the top and bottom are r_e and r_i, respectively. The distribution parameter r_0 is linearly decreased from the top to the bottom surfaces of the conic region, and it can be expressed as

$$r_0(z) = r_e - (r_e - r_i)\frac{z_e - z}{z_e - z_i} \qquad (2)$$

Through complete derivation (see Appendix), Equation 1 is of the following form
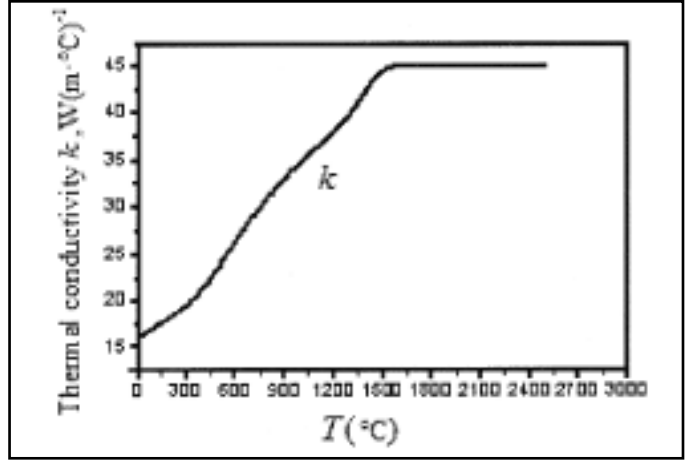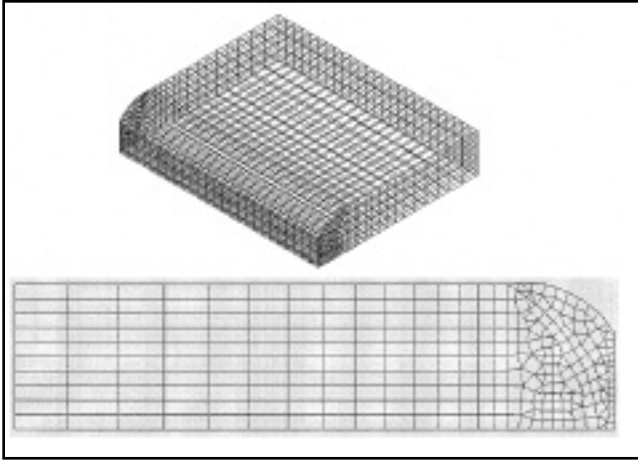
Fig. 5 — The grid system.

Fig. 6 — The thermal conductivity vs. temperature.

Table 1 — The Parameters Used for Heat Source Modes

Heat Source Modes	r_e (mm)	r_i (mm)	z_e (mm)	z_i (mm)	D_h (mm)
TDC	7.0	2.6	9.5	2.2	
MTDC	7.2	1.05	10.7	1.2	
QPAW	7.2	1.05	10.7	1.2	6.8

Table 2 — Keyhole PAW Welding Process Parameters

Case	Welding Current (A)	Arc Voltage (V)	Welding Speed (mm/min)	Plasma Gas Flow Rate (L/min)	Shielding Gas Flow Rate (L/min)
1	250	31.7	120	4	10
2	240	31.2	120	4	10

Table 3 — Comparison of the Predicted and Experimental Weld Width

Heat Source	Top Weld Width (mm)		Bottom Weld Width (mm)	
	Predicted	Measured	Predicted	Measured
TDC	13.60	14.35	4.25	2.11
MTDC	12.90	14.35	2.30	2.11
QPAW	13.90	14.35	2.30	2.11

$$Q_V(r,z) = \frac{9\eta U I e^3}{\pi(e^3 - 1)}$$

$$\times \frac{1}{(z_e - z_i)(r_e^2 + r_e r_i + r_i^2)} \exp\left(-\frac{3r^2}{r_0^2}\right) \tag{3}$$

where η is the plasma arc power efficiency, U is the arc voltage, and I is the welding current.

Modified Three-Dimensional Conical Heat Source

Although the three-dimensional conical heat source takes consideration of the heat intensity distribution and decay along the workpiece thickness, its characteristic of linear decline is not appropriate. In keyhole PAW, a bugle-like weld configuration was the result. To reflect this feature, a modified three-dimensional conical (MTDC) heat source is proposed, which is shown in Fig. 2. For the MTDC heat

source, the distribution parameter r_0 decreases no longer as linearly as for TDC, but in a curvilinear way.

As shown in Fig. 2, the height of the modified three-dimensional conical (MTDC) heat source is $H = z_e - z_i$, the z-coordinates of the top and bottom surfaces are z_e and z_i, respectively, and the diameters at the top and bottom are r_e and r_i, respectively. Let r_0 represent the distribution parameter at z. r_0 is decreased nonlinearly and can be expressed as

$$r_0(z) = a\ln z + b \tag{4}$$

After complete derivation and manipulation (see Appendix), the heat intensity for MTDC can be written as

$$Q_V(r,z) = \frac{3\eta U I e^3}{\pi(e^3 - 1)} \frac{1}{A} \exp\left(-\frac{3r^2}{r_0^2}\right) \tag{5}$$

where

$$A = a^2 \begin{bmatrix} (H + z_i)\ln^2(H + z_i) \\ -z_i \ln^2 z_i \end{bmatrix} \\ -2a(a-b)\begin{bmatrix} (H + z_i)\ln(H + z_i) \\ -z_i \ln z_i - H \end{bmatrix} + b^2 H \tag{6a}$$

$$a = \frac{r_e - r_i}{\ln z_e - \ln z_i} \tag{6b}$$

$$b = \frac{r_i \ln z_e - r_e \ln z_i}{\ln z_e - \ln z_i} \tag{6c}$$

$$r_0(z) = \frac{(r_e - r_i) \times \ln(z)}{\ln(z_e) - \ln(z_i)} \\ + \frac{r_i \times \ln(z_e) - r_e \times \ln(z_i)}{\ln(z_e) - \ln(z_i)} \tag{6d}$$
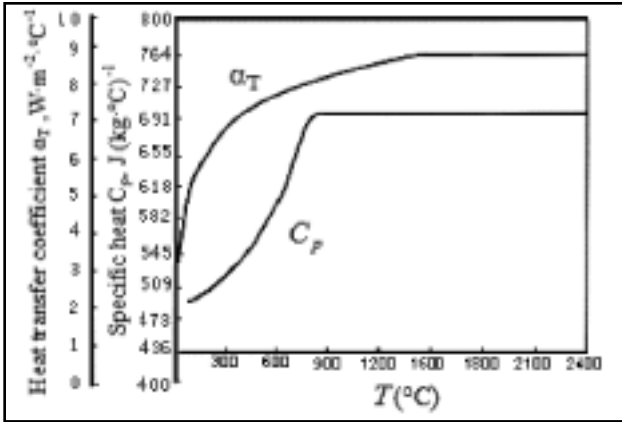
Fig. 7 — The heat transfer coefficiency and specific heat vs. temperature.
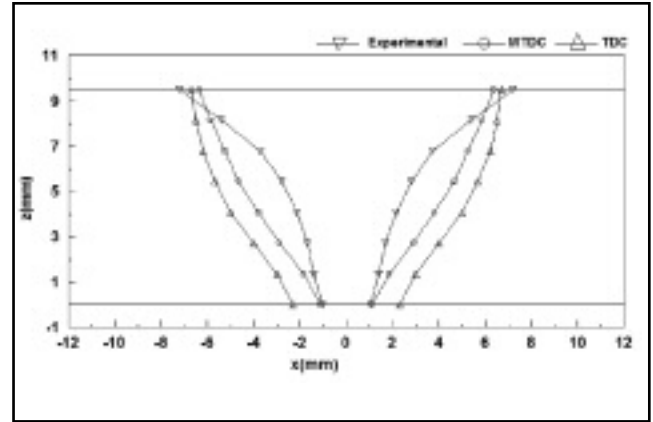

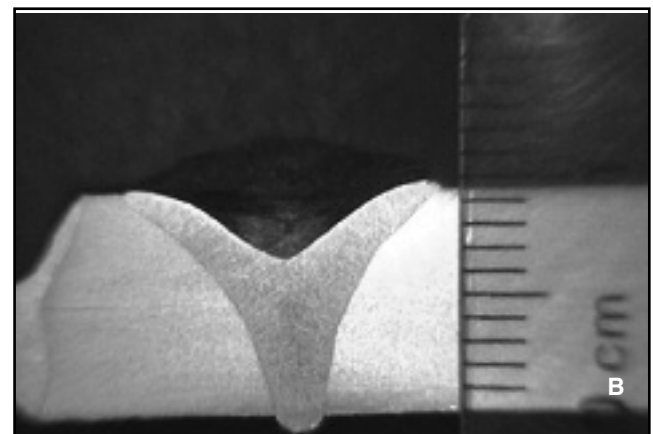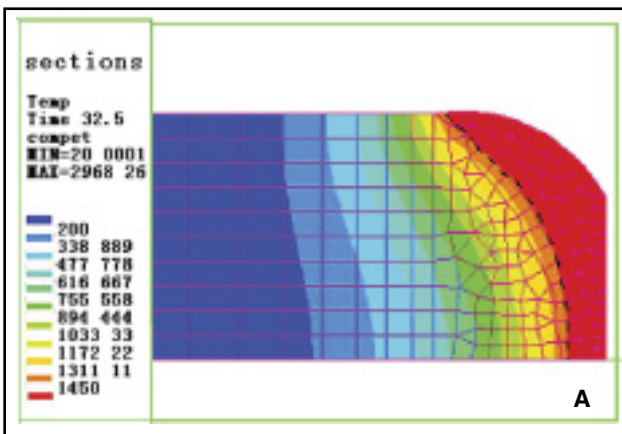*Fig. 8 — Comparison of predicted PAW cross section with experimental results.*

Fig. 9 — The cross section of a plasma arc weld under welding condition Case 1. A — The predicted result based on model QPAW; B — macrograph.

Quasi-Steady State PAW Heat Source

As aforementioned, the arc used in the PAW process is constricted by a small nozzle and has a much higher gas velocity and temperature than that in GTAW. The high plasma gas velocity and the associated momentum force the plasma jet to penetrate the base metal, forming a keyhole in the weld pool of complete penetration. Thus, the plasma jet emerges from the underbead at the bottom of the workpiece — Fig. 3. As the torch moves along the weld, this keyhole progressively cuts through the metal with the molten metal flowing behind to form the weld bead. The size and shape of the keyhole produced by PAW depend mainly on the pressure of the impinging gas. It was found that a typical plasma arc keyhole in 6-mm-thick stainless steel, 3-mm nozzle bore diameter, and 8–10 mm torch standoff is a conical hole with a circumferential diameter of 5 mm at the top and about 1.5–2 mm at the bottom end (Ref. 27). The forces that tend to form and maintain the keyhole include the plasma stream pressure, vapor pressure, and recoil pressure (Ref. 27). The existence of keyhole, on one hand, makes the heat intensity from the plasma arc distribute through the workpiece thickness, but on the other hand, causes some vaporization, which results in some heat losses. Therefore, the net heat input is not deposited on the workpiece totally. To consider this point, part of the heat density at the upper section of the keyhole is excluded. As shown in Fig. 4, the heat intensity is distributed within a domain bounded by the curves $f_0(z)$ and $f_1(z)$ at the upper section of the keyhole, while at the lower section of the keyhole, the heat intensity is distributed as a modified conical heat source. This model of heat source is proposed for the quasi-steady state PAW process, so it is referred to as QPAW for short. It can be expressed as

For the upper part, $(z_e - D_h) \leq z \leq z_e$

$$Q_V(r,z) = \frac{3\eta I U e^3}{\pi(e^3-1)A}\exp\left(-\frac{3r^2}{f_0^2(z)}\right),$$

$$f_1(z) \leq r \leq f_0(z) \tag{7}$$

where

$$f_0(z) = \frac{(r_e - r_i) \times \ln(z)}{\ln(z_e) - \ln(z_i)}$$

$$+ \frac{r_i \times \ln(z_e) - r_e \times \ln(z_i)}{\ln(z_e) - \ln(z_i)} \tag{8}$$

$$f_1(z) = \frac{r_e}{\sqrt{D_h}}\sqrt{z - z_e + D_h} \tag{9}$$

For the lower part, $z_i \leq z \leq (z_e - D_h)$, it is of the same expression as Equations 5 and 6.

FEM Analysis
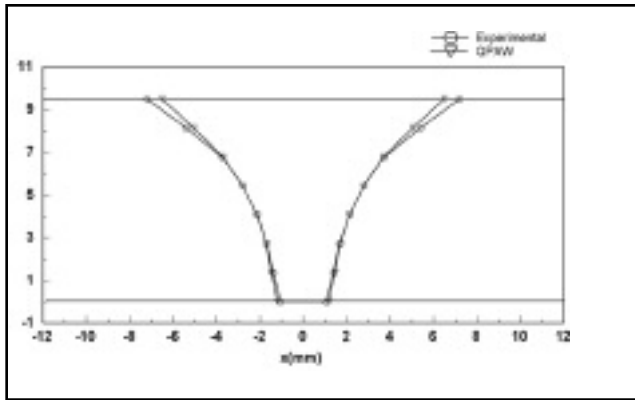
After establishing a suitable heat

Fig. 10 — Comparison between the predicted and measured weld cross section for Case 1.

Fig. 11 — The cross section of a plasma arc weld under welding condition Case 2. A — The predicted result based on model QPAW; B — macrograph.

source model for keyhole PAW, the temperature profile and weld pool geometry are able to be determined by the finite element method (FEM). In a moving coordinate system o-xyz in which the origin coincided with the intersecting point between the torch centerline and the bottom surface of workpiece, x-axis along the welding direction and z-axis normal to the workpiece surface, the quasi-steady state temperature field during keyhole PAW is governed by the following equation

$$\rho C_P \left(-v_0 \frac{\partial T}{\partial x} \right) = \frac{\partial}{\partial x}\left(k \frac{\partial T}{\partial x} \right)$$
$$+ \frac{\partial}{\partial y}\left(k \frac{\partial T}{\partial y} \right) + \frac{\partial}{\partial z}\left(k \frac{\partial T}{\partial z} \right) + Q_V \tag{10}$$

where ρ is density, C_P is specific heat, v_0 is welding speed, T is temperature, k is thermal conductivity, and Q_V is volumetric heat source. The boundary conditions for Equation 10 are as follows:

On the workpiece surface,

$$-k\frac{\partial T}{\partial z} = \alpha_T \left(T - T_\infty \right) \tag{11}$$

where T. is the ambient temperature, and α_T is the combined heat transfer coefficient.

At the symmetric plane xoz,

$$\frac{\partial T}{\partial y} = 0 \tag{12}$$

So only half of the workpiece is taken as the calculation domain. The workpiece dimension is 200 mm in length, 80 mm in width, and 9.5 mm in height.

The half domain is divided into 8-node hexahedrons. As aforementioned, part of heat density at the upper section of keyhole is excluded because of evaporation loss and keyhole effect. To reflect this characteristic and match the distribution mode of heat source QPAW, some elements in the upper section of the keyhole are treated as "dead." The discrete grids are shown in Fig. 5.

Results

The workpiece material is stainless steel 304. Its thermal conductivity k, specific heat C_P, and the combined heat transfer coefficient α_T are shown in Figs. 6 and 7. Its density is ρ = 7860 (kg m⁻³), and ambient temperature is T. = 300 K. The parameters used for describing heat source modes are given in Table 1. Keyhole PAW experiments are conducted under two welding conditions (Table 2). The arc power efficiency η takes a value of 0.66 based on the literature (Ref. 3). After welding, a macrograph of the weld is made to show its cross section.

Firstly, two kinds of volumetric heat source models, i.e., three-dimensional conical (TDC) and modified three-dimensional conical (MTDC), are used to predict the plasma arc weld geometry. Figure 8 shows the comparison of the experimental results with the predicted ones based on different models. Table 3 gives the data of weld width. From the point of view of agreement, the calculation precision of TDC is poorer. It can be seen that TDC is not suitable for determining keyhole plasma arc weld dimensions. Though the precision of MTDC is improved compared to TDC, especially the weld width at both top and bottom surfaces, the calculation precision for the location and locus of the melt-line in the weld cross section is still lower.
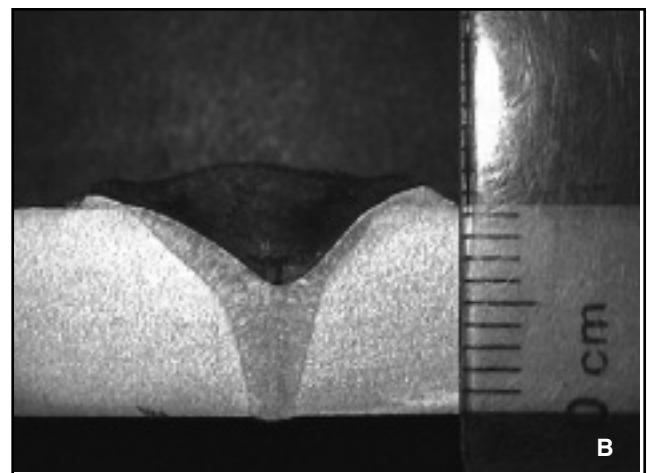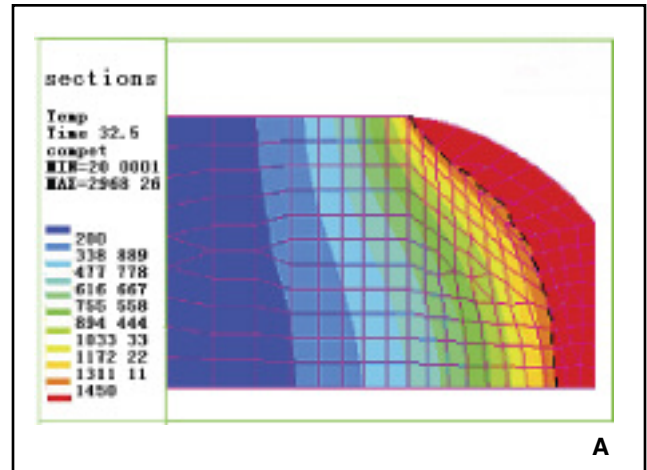
Secondly, the developed heat source model for quasi-steady state keyhole PAW, i.e., QPAW, is employed to calculate the weld geometry. Figures 9–12 show the comparison of experimental results with the predicted ones based on QPAW model for welding conditions Case 1 and Case 2, respectively. In Figs. 9A and 11A, the dotted lines are drawn along the isotherm of melting temperature. It can be seen that the predicted weld geometry agrees well with experimental measurements. Since the model QPAW depicts the character of the keyhole PAW process through considering the "bugle-like" configuration of the keyhole and the decay of heat intensity distribution of the plasma arc along the direction of the workpiece thickness, the calculation precision of the weld geometry at the cross section is quite satisfactory.

Conclusion

Because of the keyhole effect, a plasma arc weld has a large penetration-to-width ratio. For numerical analysis of welding temperature profile in keyhole PAW, an
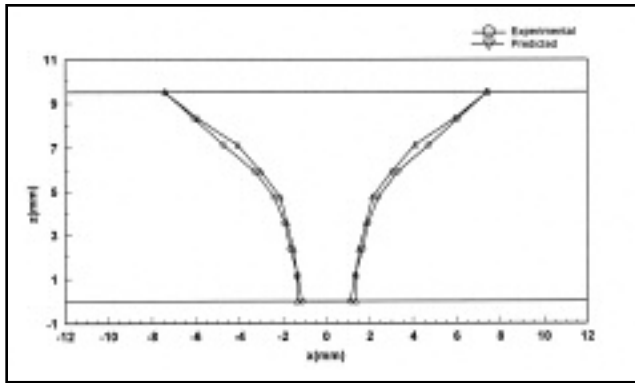
Fig. 12 — Comparison between the predicted and measured weld cross section for Case 2.

appropriate heat source model must be developed to consider the high-speed plasma jet and the associated strong momentum acted to the weld pool and the distribution of heat intensity along the direction of the workpiece thickness. Because neither the double-ellipsoidal mode of the heat source nor the three-dimensional conical mode of the heat source can be appropriate for the finite element analysis of the keyhole PAW process, a modified three-dimensional conical heat source model (MTDC) is put forward to reflect the nonlinear decay of heat intensity distribution along the direction of the workpiece thickness. Although MTDC can be used to calculate the weld width on both the top and the bottom surfaces of the workpiece, for the location and locus of the melt-line in the weld cross section, its calculating precision is lower.

A new heat source model for the quasi-steady state keyhole PAW, i.e., QPAW, is proposed, which depicts the characteristic of the keyhole PAW process quite well, because it considers both the "bugle-like" configuration of the keyhole, and the decay of heat intensity distribution of the plasma arc along the direction of the workpiece thickness. The QPAW heat source model is applied in finite element analysis of the temperature field. The results show that the calculated weld geometry at the cross section is in good agreement with the experimental one.

References

1. Graig, E. 1988. The plasma arc welding — A review. *Welding Journal* 67(2): 19–25.
2. Tomsic, M., and Barhost, S. 1984. Keyhole plasma arc welding of aluminum with variable polarity power. *Welding Journal* 63(2): 25–32.
3. Metcalfe, J. C., and Quigley, M. B. C. 1975. Heat transfer in plasma-arc welding. *Welding Journal* 54(3): 99-s to 103-s.
4. Lancaster, J. F. 1984. *The Physics of Welding*, chapter 8, Perganon Press, Oxford.
5. Metcalfe, J. C., and Quigley, M. B. C. 1975. Keyhole stability in plasma arc welding. *Welding Journal* 54(11): 401-s to 404-s.
6. Martikainen, J. K., and Moisio, T. J. I. 1993. Investigation of the effect of welding parameters on weld quality of plasma arc keyhole welding of structural steels. *Welding Journal* 72(7): 329-s to 340-s.
7. Vilkas, E. P. 1991. Plasma arc welding of exhaust pipe system components. *Welding Journal* 70(4): 49–52.
8. Irving, B. 1997. Why aren't airplanes welded? *Welding Journal* 76(1): 34–41.
9. Irving, B. 1992. Plasma arc welding takes on the advanced solid rocket motor. *Welding Journal* 71(12): 49-52.
10. Nunes, A. C. 1984. Variable polarity plasma arc welding on the space shuttle external tank. *Welding Journal* 63(9): 27–35.
11. Keanini, R. G., and Rubinsky, B. 1990. Plasma arc welding under normal and zero gravity. *Welding Journal* 69(6): 41–50.
12. Zhang, Y. M., and Liu, Y. C. 2003. Modeling and control of quasi-keyhole arc welding process. *Control of Engineering Practice* 11(12): 1401–1411.
13. Liu, Y. C. 2004. Control of dynamic keyhole welding process. PhD thesis. University of Kentucky.
14. Chen, K. X, Li, H. Q., and Li, C. X. 2004. Survey of variable polarity plasma arc welding. *Transactions of the China Welding Institution* 25(1): 124–128.
15. Zhang, Y. M., and Zhang, S. B. 1999. Observation of the keyhole during plasma arc welding. *Welding Journal* 75(2): 53-s to 59-s.
16. Dong, C. L, Wu, L., and Shao, Y. C. 2000. The history and present situation of keyhole plasma arc welding. *Chinese Mechanical Engineering* 11(5): 577–581.
17. Hsu, Y. F., and Rubinsky, B. 1987. Transient melting of a metal plate by a penetrating plasma arc. *ASME J Heat Transfer* 109(5): 463–469.
18. Hsu, Y. F., and Rubinsky, B. 1988. Two-dimensional heat transfer study on the keyhole plasma arc welding process. *Int. J Heat Mass Transfer* 31(7):1409–1421.
19. Nehad, A. K. 1995. Enthalpy technique for solution of Stefan problems: Application to the keyhole plasma arc welding process involving moving heat source. *Int. Comm. Heat Mass Transfer* 22(6): 779–790.
20. Keanini, R. G., and Rubinsky, B. 1993. Three-dimensional simulation of the plasma arc welding process. *Int. J Heat Mass Transfer* 36(13): 3283–3298.
21. Fan, H. G., and Kovacevic, R. 1999. Keyhole formation and collapse in plasma arc welding. *J Phys D: Appl. Phys.* 32: 2902–2909.
22. Kou, S., and Wang, Y. H. 1986. Computer simulation of convection in moving arc weld pools. *Metall. Trans.* 17A: 2271–2277.
23. Fan, H. G., Na, S. J., and Shi, Y. W. 1997. Mathematical model of arc in pulsed current gas tungsten arc welding. *J Phys D: Appl. Phys.* 30: 94–102.
24. Wu, C. S., and Yan, F. 2004. Numerical simulation of transient development and diminution of weld pool in gas tungsten arc welding. *Modeling and Simulation in Materials Science and Engineering* 13: 13–20.
25. Goldak, J., Chakravarti, A., and Bibby, M. 1984. A new finite element model for welding heat sources. *Metall. Trans. B* 15(6): 299–305.
26. Wang, H. X., Wu, C. S., and Zhang, M. X. 2005. Finite element method analysis of temperature field in keyhole plasma arc welding. *Transactions of the China Welding Institution* 26(7): 49–53.
27. Bertoluzzo, G. O. 1996. Plasma variable polarity pulsed arc welding 12.7 mm thick aluminium. *Proc of IIW Asian Pacific Welding Conference*, Auckland, New Zealand. pp. 875–896.

Appendix 1

Derivation for Heat Intensity Distribution Equations

For a volumetric distribution of heat intensity, the following assumptions are made:

1) The heat intensity deposited region is maximum at the top surface of workpiece, and is minimum at the bottom surface of workpiece.

2) Along the thickness of the workpiece, the diameter of the heat density distribution region is decreased in some way. But the heat density at the central axis (z-direction) is kept constant.

At any plane perpendicular to z-axis, the heat intensity distribution may be written as

$$Q_V(r,z) = Q_0 \exp\left(-\frac{3r^2}{r_0^2}\right) \quad \text{(A1)}$$

where Q_0 is the maximum value of heat intensity, r_0 is the distribution parameter, and r is the radial coordinate. The key

problem is how to determine the parameters Q_0 when the decay rule of r_0 is known.

Because of thermal energy conservation, we have

$$\eta UI = \int_0^H \int_0^{2\pi} \int_0^{r_0} Q_V(r,z)r\,dr\,d\theta\,dh$$

$$= \int_0^H \int_0^{2\pi} \int_0^{r_0} Q_0 \exp\left(-\frac{3r^2}{r_0^2}\right)r\,dr\,d\theta\,dh$$

$$= -\frac{\pi Q_0}{3}\int_0^H r_0 \int_0^{r_0} \exp\left(-\frac{3r^2}{r_0^2}\right)d\left(-\frac{3r^2}{r_0^2}\right)dh$$

$$= \frac{\pi Q_0\left(1-e^{-3}\right)}{3}\int_0^H r_0^2\,dh \tag{A2}$$

where η is the plasma arc power efficiency, U is the arc voltage, and I is the welding current.

Three-Dimensional Conical Heat Source (TDC)

As shown in Fig. 1, r_0 decreases linearly for TDC. The height of the conical heat source is $H = z_e - z_i$, the z-coordinates of the top and bottom surfaces are z_e and z_i, respectively, and the diameters at the top and bottom are r_e and r_i, respectively. The distribution parameter r_0 can be expressed as

$$r_0(z) = r_e - (r_e - r_i)\frac{z_e - z}{z_e - z_i} \tag{A3}$$

or

$$r_0^2 = \left[r_i + (r_e - r_i)\frac{h}{H}\right]^2, \quad h = z - z_i \tag{A4}$$

Since

$$\int_0^H r_0^2\,dh = \int_0^H \left[r_i + (r_e - r_i)\frac{h}{H}\right]^2 dh = \frac{H}{3}\times\left(r_e^2 + r_e r_i + r_i^2\right) \tag{A5}$$

Substituting A5 into A2, then

$$\eta UI = \frac{\pi Q_0 H\left(1-e^{-3}\right)}{9}\left(r_e^2 + r_e r_i + r_i^2\right)$$

$$Q_0 = \frac{9\eta UI e^3}{\pi\left(e^3 - 1\right)}\times\frac{1}{H\left(r_e^2 + r_e r_i + r_i^2\right)} \tag{A6}$$

Finally, substituting A6 into A1, we get

$$Q_V(r,z) = \frac{9\eta UI e^3}{\pi\left(e^3 - 1\right)}$$

$$\times\frac{1}{(z_e - z_i)\left(r_e^2 + r_e r_i + r_i^2\right)}\exp\left(-\frac{3r^2}{r_0^2}\right) \tag{A7}$$

Modified Three-Dimensional Conical Heat Source

As shown in Fig. 2, the height of the modified three-dimensional conical (MTDC) heat source is $H = z_e - z_i$, the z-coordinates of the top and bottom surfaces are z_e and z_i, respectively, and the diameters at the top and bottom are r_e and r_i, respectively. Let r_0 represents the distribution parameter at z. r_0 can be expressed as

$$r_0(z) = a\ln z + b \tag{A8}$$

Because

$$r_i = a\ln z_i + b$$

$$r_e = a\ln z_e + b$$

thus

$$a = \frac{r_e - r_i}{\ln z_e - \ln z_i} \tag{A9}$$

$$b = \frac{r_i \ln z_e - r_e \ln z_i}{\ln z_e - \ln z_i} \tag{A10}$$

Substituting A9 and A10 into A8,

$$r_0(z) = \frac{(r_e - r_i)\times\ln(z)}{\ln(z_e) - \ln(z_i)}$$

$$+\frac{r_i \times\ln(z_e) - r_e \times\ln(z_i)}{\ln(z_e) - \ln(z_i)} \tag{A11}$$

Let $h = z - z_i$. Since

$$\int_0^H r_0^2\,dh = \int_0^H (a\ln z + b)^2 dh = \int_0^H \left[a\ln(h + z_i) + b\right]^2 dh$$

$$= a^2\int_0^H \ln^2(h + z_i)\,dh + 2ab\int_0^H \ln(h + z_i)\,dh + b^2 H \tag{A12}$$

Based on the *Mathematics Handbook*,

$$\int \ln u\,du = u\ln u - u + C$$

$$\int \ln^2 u\,du = u\ln^2 u - 2\int\ln u\,du = u\ln^2 u - 2(u\ln u - u) + C$$

$$\int_0^H r_0^2\,dh = a^2\int_0^H \ln^2(h + z_i)\,dh + 2ab\int_0^H \ln(h + z_i)\,dh + b^2 H$$

$$= a^2\left[(h + z_i)\ln^2(h + z_i) - 2(h + z_i)\ln(h + z_i) + 2(h + z_i)\right]\Big|_0^H$$

$$+2ab\left[(h + z_i)\ln(h + z_i) - (h + z_i)\right]\Big|_0^H + b^2 H$$

$$= a^2\left[(H + z_i)\ln^2(H + z_i) - z_i\ln^2 z_i\right]$$

$$-2a(a - b)\left[(H + z_i)\ln(H + z_i) - z_i\ln z_i - H\right] + b^2 H$$

Let

$$A = \int_0^H r_0^2\,dh = a^2\left[(H + z_i)\ln^2(H + z_i) - z_i\ln^2 z_i\right]$$

$$-2a(a - b)\left[(H + z_i)\ln(H + z_i) - z_i\ln z_i - H\right] + b^2 H \tag{A13}$$

Substituting A13 into A2

$$\eta UI = \frac{\pi Q_0\left(1 - e^{-3}\right)}{3}\int_0^H r_0^2\,dh = \frac{\pi Q_0\left(1 - e^{-3}\right)}{3}A$$

$$Q_0 = \frac{3\eta UI e^3}{A\left(e^3 - 1\right)} \tag{A14}$$

Substitute A14 into A1, we obtain

$$Q_V(r,z) = \frac{3\eta UI e^3}{A\pi\left(e^3 - 1\right)}\exp\left(-\frac{3r^2}{r_0^2}\right) \tag{A15}$$

Appendix 2 — Nomenclature

a variable, defined in Equation A9

A variable, defined in

Equation A13

b	variable, defined in Equation A10	r	tion function $\sqrt{x^2 + y^2}$
C_P	specific heat	r_0	radial coordinate in heat source mode
D_h	variable, defined in Fig. 4	r_e	variable, defined in Figs. 1, 2, 4
e	base of natural lagarithm	r_i	variable, defined in Figs. 1, 2, 4
f_0	function, defined in Fig. 4	T	temperature
f_1	function, defined in Fig. 4	$T_\bullet$	ambient temperature
		U	arc voltage
h	$z - z_i$	v_0	welding speed
H	$z_e - z_i$	x, y, z	coordinate
k	thermal conductivity	z_e	variable, defined in Figs. 1, 2, 4
Q_0	maximum value of heat intensity	z_i	variable, defined in Figs. 1, 2, 4
Q_v	heat intensity distribu	α_T	heat loss coefficient

η	arc power efficiency
θ	angular variable
ρ	density

WELDING JOURNAL
Instructions and Suggestions for
Preparation of Articles

Text
- approximately 1500–3500 words in length
- submit hard copy
- submissions via disk or electronic transmission — preferred format is Mac but common PC files are also acceptable
- acceptable disks include floppy, zip, and CD.

Format
- include a title
- include a subtitle or "blurb" highlighting major point or idea
- include all author names, titles, affiliations, geographic locations
- separate paper into sections with headings

Photos/Illustrations/Figures
- glossy prints, slides, or transparencies are acceptable
- black and white and color photos must be scanned at a minimum of 300 dpi
- line art should be scanned at 1000 dpi
- photos must include a description of action/object/person and relevance for use as a caption
- prints must be a minimum size of 4 in. x 6 in., making certain the photo is sharp
- do not embed the figures or photos in the text
- acceptable electronic format for photos and figures are EPS, JPEG, and TIFF. TIFF format is preferred.

Other
- illustrations should accompany article
- drawings, tables, and graphs should be legible for reproduction and labeled with captions
- references/bibliography should be included at the end of the article

Editorial Deadline
- January issue deadline is November 11
- February issue deadline is December 10
- March issue deadline is January 13
- April issue deadline is February 10
- May issue deadline is March 10
- June issue deadline is April 9
- July issue deadline is May 12
- August issue deadline is June 13
- September issue deadline is July 11
- October issue deadline is August 11
- November issue deadline is September 12
- December issue deadline is October 10

Suggested topics for articles
- case studies, specific projects
- new procedures, "how to"
- applied technology

Mail to:
Andrew Cullison
Editor, Welding Journal
550 NW LeJeune Road
Miami, FL 33126
(305) 443-9353, ext. 249; FAX (305) 443-7404
cullison@aws.org